# ELLIPSOMETRY AS A PROBE OF THIN COPOLYMER FILMS: CRYSTALLISATION & MORPHLOGY

# ELLIPSOMETRY AS A PROBE OF THIN COPOLYMER FILMS: CRYSTALLISATION & MORPHLOGY

By

JESSICA L. CARVALHO

B.Sc. (McMaster University) 2004

A Thesis

Submitted to the School of Graduate Studies

In Partial Fulfilment of the Requirements

for the Degree

Master of Science

McMaster University

MASTER OF SCIENCE (2004)
(Physics)

McMaster University
Hamilton, Ontario

TITLE: Ellipsometry as a Probe of Thin Copolymer Films: Crystallisation & Morphology

AUTHOR: Jessica L. Carvalho

SUPERVISORS: Dr. K. Dalnoki-Veress

NUMBER OF PAGES: vii, 49

# Abstract

This study presents results on the use of ellipsometry as a novel probe for thin films of a diblock copolymer. Ellipsometry makes use of the change in polarisation induced upon reflection of light from a film covered substrate to enable calculation of the refractive index and thickness of the film. The information obtained in these measurements can be compared to differential scanning calorimetry, with the additional advantages that small sample volumes and slow cooling rates can be employed, and expansion coefficients can be determined. The work is presented in two parts; first crystallisation within the phase-separated domains is studied, then a morphological transition in the diblock ordering is characterised. By studying the temperature dependence of the film thickness and refractive index, crystallisation kinetics within very small volumes (~ $10^{-10}$ L) of a poly (butadiene-b-ethylene oxide) diblock copolymer are measured. Through a comparison of two different PEO block lengths, a reduction in both the crystallisation and melting temperatures is demonstrated as the domain volume is decreased. Upon cooling, an additional transition is observed. We ascribe this to a morphological transition from a layer of ordered spheres to a lamellar layer at the substrate, which is consistent with a comparison between the data and simulated ellipsometry data. The sensitivity of ellipsometry makes it a well suited and versatile technique for probing thin film kinetics in diblock copolymers.

# Acknowledgements

The last two years have been a learning experience to say the least, and it has taken an army of support to see me to the end of this. I would first like to thank Kari Dalnoki-Veress for being not only a superb supervisor, but a mentor and friend as well. I've learned more from you than I could from any textbook, and your enthusiasm and guidance has kept me moving in the right direction time and time again.

Endless thanks goes to my labmates: Mike (a.k.a. mini-supervisor…both figuratively and literally!) for patiently putting up with all my embarrassingly stupid questions and brain-lapses, and from whose example I've learned how to be an experimentalist. This thanks is also extended to Adam, Andrew, Marie-Josée, Matt and Joe, and all the former students of this lab, for the long conversations, brainstorming, imparted wisdom and experience, Simpson's lunches and the fun we've had in between. I thank Laura who helped make suffering through courses more tolerable, and for the good times we've had as friends.

A very special thanks is extended to my family and friends. In particular, the support and encouragement from my mom and dad has gone beyond the call of duty as parents. I don't think I could ever properly thank you guys for all you've given me. And of course, a thank you goes to my sister, Jen, without whose love and friendship I would be lost. Thanks for keeping me cultured!

Finally, last but most certainly not least, there is my partner in crime, Jamie. I could not have gotten to this point without your endless support, understanding, dedication and love. I could never thank you enough for standing by me and for patiently putting up with me all these years!

Jessica Carvalho

# Contents

# List of Figures

# Chapter 1

# Introduction

## 1.1 Polymers

Polymers are part of a large class of materials known as *soft condensed matter.* Soft materials share some rather unique properties such as their remarkable tendency toward self-assembly, making them interesting from a technological point of view. Given their widespread use, an understanding of the properties inherent to these materials is important. Polymer chains are commonly referred to as *macromolecules*, because the large number of molecular units, $N$. These units are called monomers, and they are covalently linked together to form a polymer chain. Typically, a single chain is built from a very large number of monomers ($N >> 1$). Polymers synthesized in the lab will usually have $N \sim 10^2 - 10^4$, whereas natural polymers can be much longer. For example DNA, one of the longest known polymers, has $N \sim 10^9 - 10^{10}$ [1].

### 1.1.1 Molecular Architecture

Most polymers are carbon based, thus the synthesis of polymers is a branch of organic chemistry. Poly(ethylene) has one of the most basic chemical structures, comprised of a main chain of single-bonded carbon atoms, with 2 additional hydrogen atoms per carbon atom (Figure 1.1). Other polymer chains may involve additional side groups, branching, networking, and numerous other atoms besides carbon and hydrogen,

resulting in more complex structure and chemistry. The particular shape the molecule takes is referred to as its *molecular architecture*, with the simplest structure being the linear chain, like the polyethylene molecule described previously. In Figure 1.2, some possible architectures are shown schematically. For example, the ends of a linear chain can be permanently fixed together to form a loop. Branching off the main chain can result in short- or long-chain branched, star-branched or ladder structure. Crosslinking of different chains results in networks and dendrimer architectures. A polymer's molecular architecture greatly affects its physical properties.

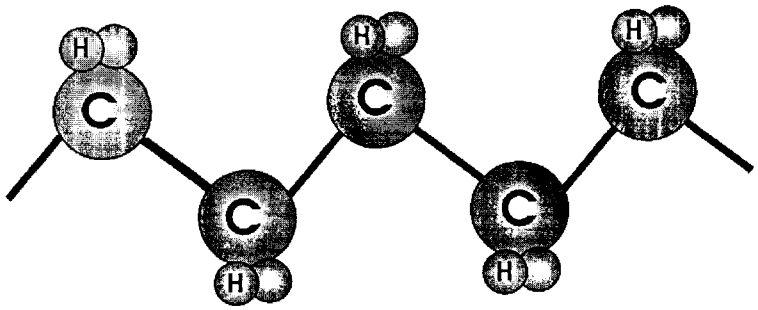


Figure 1.1: Linear structure of poly(ethylene).

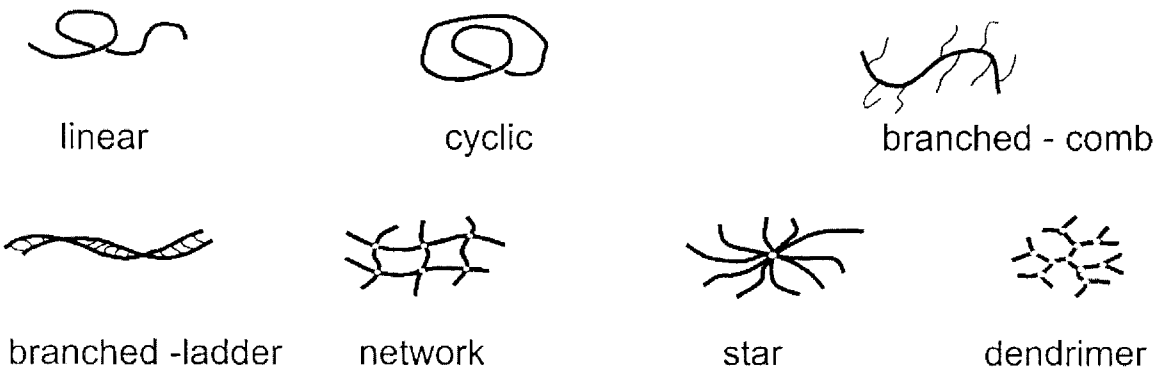


Figure 1.2: Various polymer configurations.

### 1.1.2 Tacticity

The way side groups are arranged along the main chain in three dimensions is referred to as the molecule's *stereochemistry*. The term *tacticity* describes the steric order of a chain. A molecule's tacticity effects whether the molecule can crystallise or will simply form a glass upon cooling. There are two regular arrangements of the side groups and one random, as seen in Figure 1.3. *Isotactic* polymers have a regular arrangement of side groups in which they appear on the same side of the chain. Polymers which are *syndiotactic* exhibit side groups on alternate sides of the chain in a regular manner. Finally, *atactic* polymers have their side groups arranged in a completely random way.

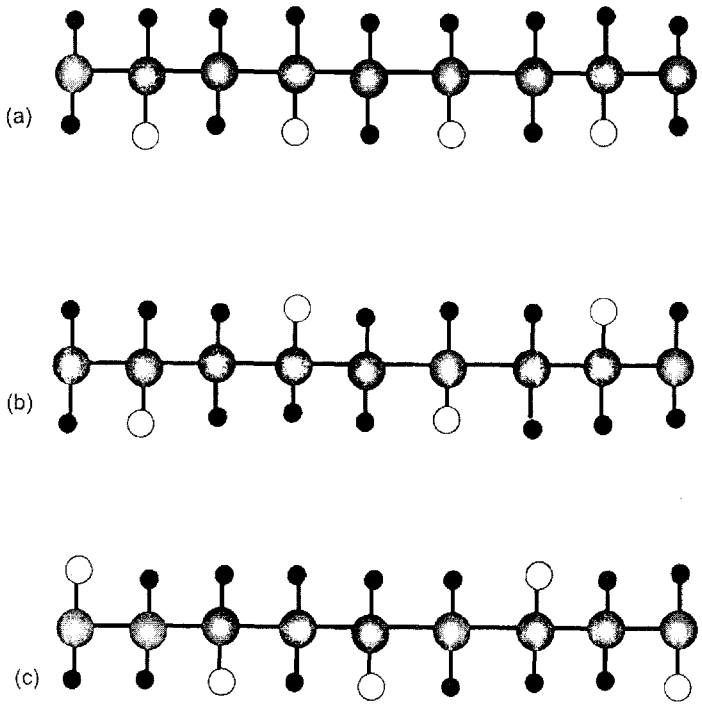


Figure 1.3: Schematic of polymer stereochemistry. (a) Isotactic and (b) syndiotactic forms involve a regular arrangement of the sidegroups, as opposed to the (c) random tacticity arrangement.

### 1.1.3 Conformations

The atoms of the molecules themselves are not rigidly fixed in equilibrium positions. Thermal collisions between the polymer molecules themselves or with solvent molecules allow for oscillations about these equilibrium positions. This may lead to rotations and deformations of the bond angles. One can visualise the effect these rotations and deformations have by thinking of a single polymer chain as a construction of rigid segments attached by somewhat flexible joints. On very small scales, this section of rods may appear rigid. However, as one goes to larger scales, the rotations and deformations become additive along the chain, resulting in a very flexible, coiled molecule [1] (see Figure 1.4).

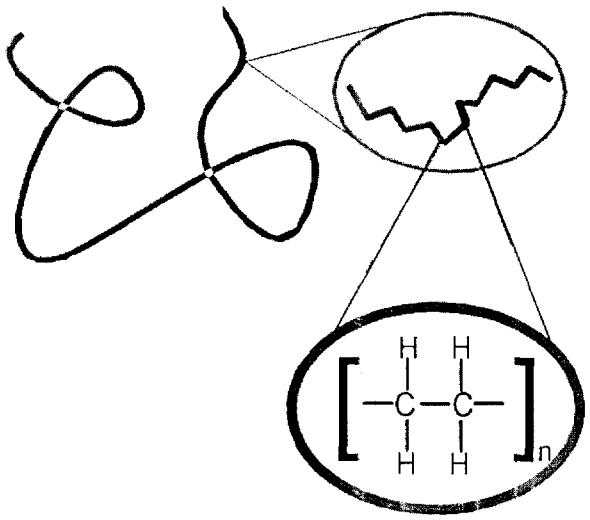


Figure 1.4: Schematic depicting various lengthscales relevant to chain flexibility. On the smallest lengthscale of a few monomers (styrene in this case), chain segments are quite rigid. On larger lengthscales, oscillations add up to a coiled, flexible polymer chain.

### 1.1.4 Molecular Weight

The size of a polymer can be characterized through its molar mass. A polymer's molecular mass affects many physical properties. For example, very low molar mass molecules (referred to as *oligimers*), show a strong increase in melting temperature with increasing molar mass. Similar dependencies are found for other properties such as fracture toughness and Young's modulus [2]. Generally, synthetic polymers show a broad molar mass distribution, which in some cases can range three or four orders of magnitude, due to the difficulty for synthesis methods to yield molecules of identical length [2]. The size of this distribution range is characterized by the *polydispersity index*, $\overline{M}_w/\overline{M}_n$. Here, $\overline{M}_n$ is the number average molecular mass [2]:

$$\overline{M}_n = \frac{\sum_i N_i M_i}{\sum_i N_i} = \sum_i n_i M_i ; \tag{1.1}$$

and $\overline{M}_w$ is the weight average molecular mass [2]:

$$\overline{M}_w = \frac{\sum_i N_i M_i^2}{\sum_i N_i M_i} = \frac{\sum_i W_i M_i}{\sum_i W_i} = \sum_i w_i M_i ; \tag{1.2}$$

where $N_i$ is the number of molecules of molar mass $M_i$, and $n_i$ is the numerical fraction of those molecules, $W_i$ is the mass of the molecules of molar mass $M_i$, and $w_i$ is the mass fraction of those molecules. A perfectly monodisperse polymer sample has $\overline{M}_w/\overline{M}_n = 1$, meaning every chain has identical molar mass; otherwise it is always the case that $\overline{M}_w/\overline{M}_n > 1$.

### 1.1.5 The Size of a Random Chain

There are two common ways of describing the size of a random polymer chain, the *root-mean-square end-to-end distance* or the *radius of gyration*. The actual fully extended chain length does not have much use in describing the size of a chain. This is because, it is not entropically favourable for chains to remain fully extended, with the preference being an entangled, coiled state. In the melt or at theta temperatures in a solvent, the chain distribution can be described as a random walk with a Gaussian distribution function. These chains are referred to as being Gaussian or ideal. Thus, the root-mean-square end-to-end distance, $\bar{r}$, is often used to describe chain size, which is simply the distance between the ends of the chains. $\bar{r}$ scales with the square root of the mass of the polymer [2]:

$$\bar{r} = l(N)^{1/2}; \tag{1.3}$$

where we have considered a chain with $N$ segments of length $l$. This result follows from random walk statistics. On the other hand, the radius of gyration, $\bar{R}_g$, measures the root-mean-square distance of a collection of molecules from their common centre of gravity. Debye showed that for large linear molecules (large $N$), like polymers, the radius of gyration scales with the end-to-end distance [2]:

$$\langle \bar{R}_g \rangle = \langle \bar{r}^{\,2} \rangle / 6; \tag{1.4}$$

Both these measures are useful in characterising the size of a random polymer, where by random it is meant that there are no correlations between monomers on distances greater than these statistical lengths.

## 1.2 Polymer States

It is common to think of materials as existing in three states of matter: solid, liquid or gas (four, if one considers the much rarer plasma phase). The unique macromolecular nature of polymers, however, affects the physical states possible for polymeric materials.

Due to the high molecular weight of most polymers, the gas phase is unattainable. The plasma phase occurs at temperatures so high that the bonds holding the molecules of the chains together cannot exist. While, solid and liquid phases are common for polymers, they come with some very unique properties. There are four physical states that polymeric systems are most commonly found in: liquid, glassy, crystalline and liquid crystalline.

### 1.2.1 Polymer Liquids

Pure polymers in the liquid state are referred to as the *melt*. This state consists of a collection of Gaussian chains, which for longer chains will be highly entangled. Polymers in this state are also called *amorphous*. Polymeric fluids are known for their high viscosity and exhibit the unusual property of *viscoelasticity*. They exhibit a viscous response to slowly changing forces, behaving like a low molecular weight simple fluid, or an elastic response to quickly varying forces, behaving like an elastic solid. Viscoelasticity can be understood from the point of view of *entanglements*. Polymer molecules are very long objects that cannot pass through each other. In the fluid state one will have a mass of extended, interpenetrating chains, much like a pot of spaghetti. Chain entanglements within the melt oppose fluid flow. Thus, on long timescales, the behaviour of the chains is that of a viscous fluid since the chains must first disentangle before the melt can flow. On shorter timescales, entanglements behave like temporary crosslinks, resulting in elastic behaviour. Properties of the molten state are more dependent on molar mass than any other physical state since the randomly coiled chains experience higher degrees of entanglement as molar mass is increased [2].

The motion of a single chain within the melt is believed to occur via a process called *reptation*. If we consider a single chain surrounded by a sea of other chains, we can think of the molecule as being confined to a tube whose walls are constructed by the surrounding chains and thus impenetrable. When no external forces are present, the motion of the chain within the tube is purely diffusive. The chain undergoes a random

walk, allowing it to wiggle back and forth until it has escaped the tube. This snake-like motion within the tube is what is referred to as reptation [3].

### 1.2.2 Polymer Glasses

Materials that are *fully* amorphous lack sharp, crystalline Bragg scattering reflections at *any* temperature [2]. This means that if there is any order present in the material, it can only be on a very small scale and highly localised. Fully amorphous polymers are unable to crystallise due to irregular chain structures (for example, atactic or highly branched polymers and statistical copolymers). When these materials are cooled from the melt, their thermal motion is reduced. At some point, motion at the largest lengths becomes much slower than experimental timescales. This slowing of thermal motion proceeds to smaller length scales as the energy barriers for molecular motion get larger, with motion eventually restricted to only small groups of atoms. The transition to this state is known as the *glass transition*, and polymers that have undergone a glass transition are known as *polymeric glasses*. The glass transition occurs over a fairly narrow temperature range, denoted by the glass transition temperature, $T_g$. Polystyrene is a common example of a polymer that is unable to crystallise, thus forming a glass upon cooling, with $T_g \approx 100\ ^\circ$C [1]. Polymeric glasses are usually transparent. This can be attributed to the fact that they lack structure on a lengthscale comparable to the wavelength of light, thus light is able to pass through these materials easily without being scattered.

### 1.2.3 Crystalline State

Despite the melt being so highly disordered and entangled, the *crystalline* state is possible for some polymers. Polymers that can crystallise are typically referred to as being only semicrystalline, referring to the fact that the material will have regions of ordered crystalline material separated by amorphous material. Thus, they show crystalline Bragg reflections in scattering experiments superimposed on an amorphous background

[2]. There is a huge range in the degree of crystallinity achieved in these materials, with some as low as 5% crystallinity, like some poly(vinylcholrides), and others as high as 98%, such as some low molar mass polyethylenes [2]. This partial crystallinity has numerous origins: (1) long randomly entangled chains result in slow kinetics; the time to completely disentangle the chains to form a perfectly ordered crystal is beyond experimentally accessible timescales, (2) disorder is built into the polymer chains themselves (which is referred to as *quenched disorder*) through random stereochemistry and tacticity, and random sequencing, and (c) branching off the main chain can make packing into a regular crystal difficult [3].

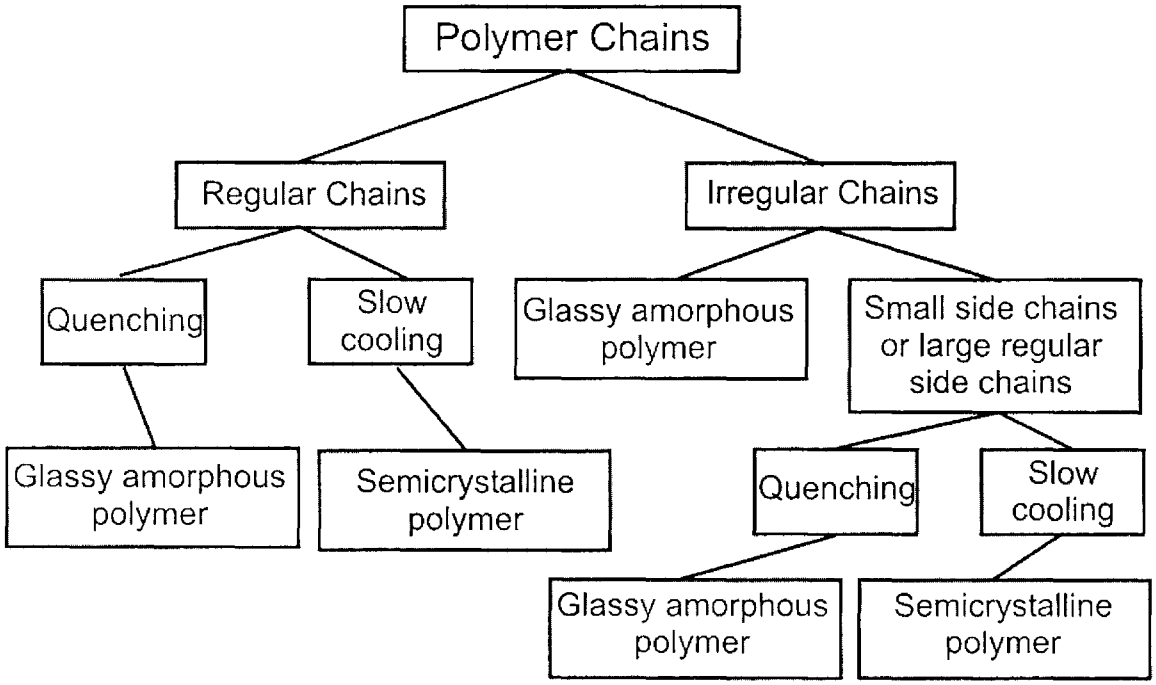


Figure 1.5: Various pathways available upon cooling a polymer melt. The final cooled state will depend on both temperature ramp rate and chain structure. Figure adopted from reference [2].

Even though a polymer may be capable of crystallising, it is possible to supercool the melt so quickly that crystal order does not have enough time to set in before the polymer reaches its glass transition temperature. In this case, the polymer simply freezes into the glassy state, bypassing the crystalline state altogether. In Figure 1.5, a flowchart indicates the different pathways a polymer melt may take upon cooling, depending on the molecular and thermal factors at play.

The *chain-folded lamella* is the basic unit from which polymer crystals are built, which are then typically organised into a *spherulite* superstructure on larger length scales (Figure 1.6). Spherulites can range many microns in size while lamellar thicknesses are on the order of 10 nm [3]. The exact lamellar thickness is a function of supercooling (ie; the final thickness is the fastest which will grow). This tendency for morphology to be kinetically driven rather than the result of equilibrium (the state of lowest free energy) is typical of polymeric systems. In most cases, the equilibrium state is experimentally unattainable. This is another interesting consequence of the macromolecular nature of polymer chains.

### 1.2.4 Liquid Crystalline State

As discussed earlier, the fourth state one may find a polymer in is the *liquid crystalline* state. Polymeric liquid crystals possess orientational order, but not positional order, intermediate between a fully amorphous and semi-crystalline phase. Changes in variables like temperature or solution concentration can allow the polymer molecules to be aligned.

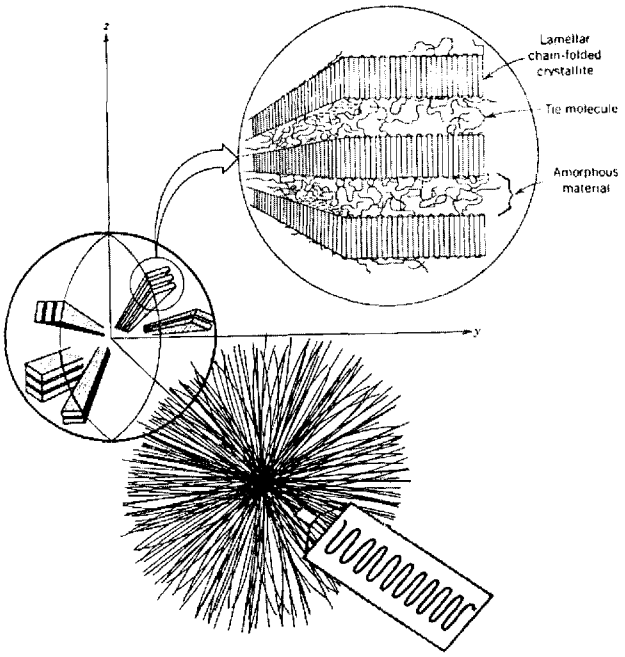


Figure 1.6: Schematic of spherulite superstructure. On the smallest lengthscale is the chain-folded lamella separated by amorphous polymeric material. Lamellae are organized into spherulites which can range a considerable spatial extent, often microns in size.

## 1.3 Phase Transitions

An understanding of the kinetics of phase transitions is essential to understand self-assembly. Phase transitions within polymer systems do not usually result in equilibrium phases. This would require a complete disentangling and rearrangement of the individual polymer chains, which would take place over a very large timescale. A system is therefore more likely to be found in a *local* free energy minimum. This can result in interesting intermediate 'kinetic' structures.

### 1.3.1 Phase Separation

When two different liquids form a homogeneous mixed phase at high temperatures but prefer to phase-separate at lower temperatures (a liquid-liquid transition), the transition can take place via two different mechanisms: *spinodal decomposition* or *nucleation and growth*. Which mechanism will take place depends on where the polymer mixture lies on its phase diagram, as determined by $\chi$ (or alternatively temperature) and the volume fraction, where $\chi$ is the Flory-Huggins parameter, representing the energy of interaction per monomer.

Spinodal decomposition is the phase-separation mechanism for systems unstable to small concentration fluctuations. Phase-separation takes place through a continuous change in composition, whereby these concentration fluctuations lower the system's free energy and are then amplified, growing continuously. This results in the flow of material from areas of low concentration to areas of high concentration. This seems counter-intuitive, as diffusion usually acts in the opposite way, towards uniform concentration. However, at equilibrium it is the chemical potential, and not concentration that must be uniform and thus material will diffuse according to the chemical potential gradient [4]. The chemical potential is related to the first derivative of free energy with respect to concentration [3]:

$$\mu = \frac{\partial}{\partial \phi}\left[ f_0(\phi) + \kappa\left(\frac{d\phi}{dx}\right)^2 \right]; \qquad (1.5)$$

where $\mu$ is chemical potential, $f_0(\phi)$ is the free energy per unit volume for a uniform mixture of composition $\phi$, and $\kappa$ is the gradient energy. Inside the spinodal region of the phase diagram, the second derivative of free energy with respect to concentration is negative. The diffusion coefficient is directly proportional to the second derivative of free energy, so the diffusion coefficient is also negative [5]. As a result, material flows from areas of low concentration to high concentration. Fluctuations in composition grow exponentially, leading to the growth of phase-separated domains [3].

The other mechanism for phase-separation is nucleation followed by growth. This is the pathway taken by systems that are stable to fluctuations in composition, provided those fluctuations are relatively small. Thus, the system cannot phase-separate via a continuous change in composition because of this stability. In terms of free energy, there is a local minimum in which the system initially resides. A large fluctuation in composition has to take place in order for the system to pass the free energy barrier and find the true minimum, meaning a domain of pure composition must be *nucleated* and subsequently grow. One can estimate the energy required to nucleate such a domain of radius $r$ as follows: by forming a droplet of pure composition, the free energy of the drop is lowered by an amount proportional to its volume, as it is favourable for molecules of the same composition to be together. However, the formation of the domain also creates an interface between the unlike polymer molecules, leading to an increase in free energy proportional to the surface area of the droplet. Thus, the net change in free energy due to nucleating a domain is [3]:

$$\Delta F(r) = \frac{4}{3}\pi r^3 \Delta F_v + 4\pi r^2 \gamma, \tag{1.6}$$

where $\Delta F_v$ is the change in free energy per unit volume, and $\gamma$ is the interfacial energy. $\Delta F(r)$ has a maximum for a critical size $r^*$:

$$r^* = \frac{-2\gamma}{\Delta F_v}; \tag{1.7}$$

Domains below this size will be unstable and incapable of growing, while domains above this size will grow, lowering the free energy of the system. The minimum free energy required to form this minimum-sized domain is:

$$\Delta F^* = \frac{16\pi\gamma^3}{3\Delta F_v^2}; \tag{1.8}$$

This calculation shows that nucleation must be *activated*. A fluctuation is required which will increase the local free energy by an amount $\Delta F^*$, occurring with a probability proportional to the Boltzmann factor ($-\Delta F^* / k_B T$) [3]. Through the growth of domains, the system can minimise the amount of interface present. Interfaces have a tension, called

the *interfacial tension*, which is equivalent to an interfacial free energy; thus by reducing the amount of interface, the system reduces its free energy.

### 1.3.2 Crystallisation

The liquid-crystal transition takes place via nucleation. To understand the kinetics of nucleation, consider a polymer in the undercooled melt (below the melting point) such that crystallisation is initiated by the spontaneous appearance of a crystal nucleus of radius $r$. Analogous to what was described for nucleated phase separation in section 1.3.1, the change in free energy $\Delta G(r)$, can be written as the sum of a surface area dependant term, representing the solid-liquid interfacial contribution, and a volume dependant term, representing the change in Gibbs free energy in going from the liquid to crystal phase [3]:

$$\Delta G(r) = \frac{4}{3}\pi r^3 \Delta G_v + 4\pi r^2 \gamma_{sl}; \tag{1.9}$$

where $\Delta G_v$ is the free energy change per unit volume in going from a liquid to a solid and $\gamma_{sl}$ is the interfacial energy. During the liquid to solid transition, a latent heat $\Delta H_m$ is released, which is related to the change in entropy upon freezing, $\Delta S_m$, by [3]:

$$\Delta S_m = \frac{\Delta H_m}{T_m} = \left(\frac{\partial G_s}{\partial T}\right)_P - \left(\frac{\partial G_l}{\partial T}\right)_P. \tag{1.10}$$

Assuming the undercooling, $\Delta T$, is small enough that over the temperature range the partial derivatives are approximately constant, the free energy change per unit volume change, $\Delta G_v$, when the melt freezes is [3]:

$$\Delta G_v = -\left(\frac{\Delta H_m}{T_m}\right)\Delta T_m; \tag{1.11}$$

Therefore, $\Delta G(r)$ can be rewritten as:

$$\Delta G(r) = -\frac{4}{3}\pi r^3 \left(\frac{\Delta H_m}{T_m}\right)\Delta T_m + 4\pi r^2 \gamma_{sl}. \tag{1.12}$$

This expression represents the change in free energy in the system when a crystal nucleus of size $r$ is spontaneously formed. This function can be maximized for a critical size $r^*$:

$$r^* = \frac{2\gamma_{sl}T_m}{\Delta H_m T_m}. \tag{1.13}$$

Thus, just as for the liquid-liquid phase transition via nucleation, crystals smaller than $r^*$ will be unstable and melt, while crystal nuclei larger than $r^*$ will continue to grow, lowering the local free energy by doing so. By substituting equation 1.13 into equation 1.12, the energy barrier that must be overcome to initiate a stable crystal nucleus is given by:

$$\Delta G^* = \frac{16}{3}\pi\gamma_{sl}^3\left(\frac{T_m}{\Delta H_m}\right)^2\frac{1}{\Delta T^2}; \tag{1.14}$$

with an associated nucleation probability proportional to [3]:

$$\exp\left(\frac{-\Delta G^*}{k_B T}\right). \tag{1.15}$$

This derivation assumed the *spontaneous* formation of a crystal nucleus (ie; formed from the polymer material itself), a process which is referred to as *homogeneous* nucleation. From equation 1.15, the probability for initiating homogeneous nucleation is very strongly dependant on temperature, with an exponential increase in probability as temperature is decreased. This is typically what is seen in the literature for polymer systems that are thought to have been nucleated homogeneously, where very large undercoolings are required to initiate nucleation [7-11].

Despite equation 1.15, which suggests a large undercooling is required to initiate crystal nucleation, in many cases nucleation is observed for only a few degrees of undercooling. In fact, these cases are initiated by what is called *heterogeneous* nucleation, a defect driven process. In heterogeneous nucleation, the presence of a surface (a contaminant particle, dust, the substrate the polymer material is being supported by, etc) acts to considerably lower the activation energy for nucleation, meaning smaller undercoolings are required to initiate nucleation. Thus, heterogeneities in the polymer

melt can dramatically increase the probability for nucleation at higher temperatures compared to the homogeneous case, as seen experimentally [7,9,11]. Nucleation in bulk polymer samples is typically achieved through defects since it is difficult to prepare samples that are completely free from heterogeneities. Through the use of microscopy techniques it is possible in many cases to confirm nucleation has occurred from a defect, with further support gained from the relatively small undercoolings required to initiate the formation of a crystal nucleus.

## 1.4 Copolymers

A *homopolymer* is the simplest polymer chain to consider and refers to a chain built from one single kind of repeating unit. It is possible to synthesize more sophisticated polymers, not just from the point of view of architecture, but also chemical complexity. A *copolymer* is a polymer made from two or more repeating units which are chemically distinct and covalently linked together. There are many ways these repeating units can be arranged along the chain, as depicted in Figure 1.7. A *random copolymer* has the repeat units arranged in a completely random way. These materials generally have properties intermediate between the properties of the individual repeating unit homopolymers. A *block copolymer* has the repeating units arranged in distinct sections. Often, these materials will phase-separate to minimize the energetically unfavourable interactions between the chemically distinct segments, leading to the formation of complex structures. *Sequenced copolymers* have the repeating units arranged in a non-periodic way, but the order is prescribed. The most common example of this is DNA and proteins, where the sequencing of the subunits is non-periodic but specific to function [3]. Copolymers made up of two subunits (A and B blocks) are referred to as a *diblock*, a *triblock* can be composed of two A blocks and one B block or three distinct blocks, and any varying number of blocks are referred to a *multiblock*. The rest of the discussion will focus on diblocks.

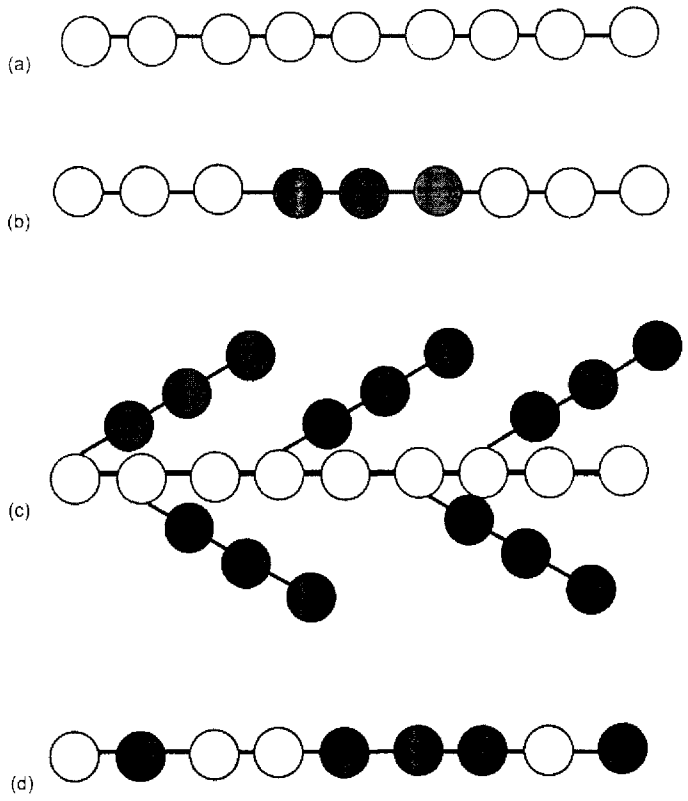


Figure 1.7: Schematic of various copolymer structures: (a) homopolymer, (b) block copolymer, (c) graft copolymer and (d) random copolymer.

### 1.4.1 Phase Separation in Block Copolymers

The compatibility of the different block segments is determined by $\chi N$. A positive $\chi$ value dictates an unfavourable interaction between A and B blocks. When $\chi N \leq 10$, entropy is favoured over the energetic penalty of mixing A and B and thus the diblock remains in a disordered homogeneous phase [12]. As $\chi N$ becomes large enough, an order-disorder transition (ODT) takes place and the blocks segregate into A- and B- rich domains. In a simple AB blend of homopolymers, A- and B- domains grow to minimize the amount of interface present. Phase separation takes place on a macroscopic scale. With diblocks, the connectivity of the blocks inhibits macroscopic phase separation. When the A and B blocks segregate, the size of the domains are limited to the size of the single blocks, resulting in nanometer dimensions. An ordered structure results since all the domains are uniform in size, arranging into a regular pattern [13].

In Figure 1.8(a), some common phase structures are shown schematically, as well as where they lie on the phase diagram (Figure 1.8(b)). The simplest structure to consider is the lamellar (L) phase, where A and B blocks are approximately the same length, resulting in alternating layers of A- and B-rich domains. The cylindrical (C) phase packs the minority component into cylinders on a hexagonal lattice. The most asymmetric volume fraction results in the spherical (S) phase, with the minority component packed into a BCC lattice of spheres. These are called the classical phases, and the most easily attained experimentally [13]. Intermediate between these are the more complex phase structures. For example, the gyroid (G) phase, which falls between L and C on the phase diagram, has the minority component forming two interweaving three-fold coordinated lattices. Less commonly found is the perforated lamellar (PL), which is actually only meta-stable [14]. The PL phases is similar to the L phase but with a hexagonal arrangement of perforations in the minority layers. Typically, this structure falls into the G phase after long enough annealing [13, 15, 16].

### 1.4.2 Block Copolymer Modelling

The most basic block copolymer model system is a pure A-b-B melt, composed simply of two sequential blocks, denoted A and B. This system is commonly modelled by the standard Gaussian model theory. This has amazingly been embraced by most researchers as the standard single model (with slight alterations, of course), with a very comprehensive review available by Matsen [13]. In this theory, high molecular weight polymers are modelled as Gaussian chains, represented by smooth space curves with

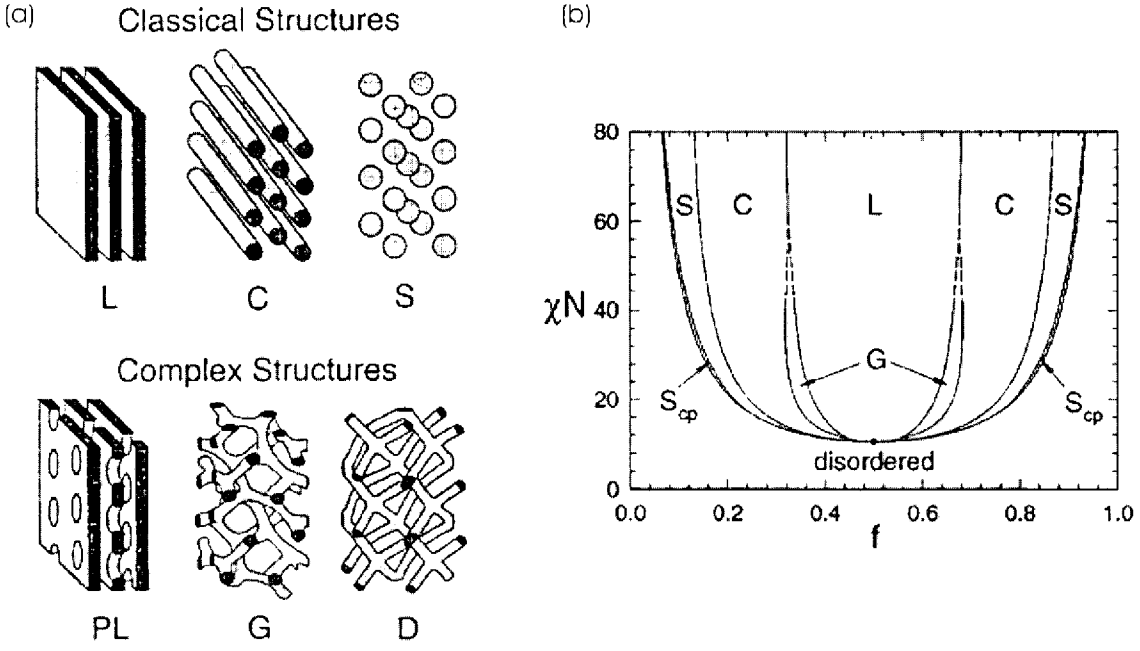


Figure 1.8: (a) Schematic of various phase-separated morphologies found for block copolymers. (b) Mean field phase diagram for block copolymer melts with phase-separated morphologies labelled. Figures taken from reference [12].

simple stretching energies to account for their local configurational entropy. A single Flory-Huggins $\chi$ parameter represents interactions between A and B segments. The model takes single chains into account, but ignores atomic structure, and has proven very accurate in comparison with experimental data for explaining block copolymer phenomena. For example, calculations accurately predict the spontaneous curvature a system will adopt given its volume fraction, producing a phase diagram similar to that found experimentally [13]. It is well known that roughly symmetric diblocks prefer flat interfaces, hence the resulting L phase. As the volume fraction becomes more asymmetric, the interface prefers to curve toward the minority block, resulting in C, G, S etc. Calculations have correctly predicted which volume fractions will result in which phases [13].

### 1.4.3 Packing Frustration

Spontaneous curvature is not the only consideration toward what final phase-separated structure results. While it is known that the interfacial energy is going to act in a way that the area is minimized under the constraint of fixed volume fraction, the stretching energy must also be considered for block copolymer melts. Thus, assuming the chains are acting as identical connected springs, they will prefer to (1) distribute their stretching energy evenly and (2) form uniformly thick brushes. However, in general they cannot satisfy both constraints simultaneously. This is what is referred to as *packing frustration* [13]. The L phase is the only phase that does not experience this frustration due to its flat curvature and constant domain thickness. For phases that have curved interfaces, there are two tendencies: Within a unit cell there will be an attempt to maintain a uniformly curved interface. Doing so, however, puts additional stress on the chains nearest to the vertices of the unit cell which will require a greater degree of stretching than chains further away. To alleviate this stress caused by the non-uniform degrees of stretching, all chains are allowed to stretch to the same amount. This, however, leads to

an increase in interfacial area. These competing tendencies must be balanced, thus there will always be some degree of packing frustration present within phases with curved interfaces [13]. The double-diamond (D) phase seen in Figure 1.8(a) has an excessive degree of packing frustration, making it unstable, which is why this phase is never actually seen in diblock systems. The PL phase also has a higher degree of packing frustration, though not quite as high as the D phase, which contributes to its meta-stability. Packing frustration also plays an important role in how the C and S phases are arranged into a lattice. The hexagonal and BCC arrangements respectively minimize this frustration, and thus are the most commonly encountered ordering for these structures. One way of relieving packing frustration within the lattice is to blend the diblock system with homopolymer corresponding to the minority block. Provided the molecular weight of the homopolymer is much smaller than its corresponding diblock molecular weight (referred to as the *wet brush* condition [17]), the homopolymer chains will mix into the diblock system and tend to accumulate at the points where frustration is strongest. They help relieve this packing frustration by allowing the excessively stretched chains to relax, while still maintaining a minimized interface.

### 1.4.4 Bulk versus Thin Films

While block copolymer phase separation has been the subject of intense research for some thirty years now, this work has been mostly centred on bulk systems [18]. Considerably less attention has been paid to thin films with more effort made in recent years. In the bulk, morphologies most often consist of "grains" of ordered domains, much like for atomic crystals, where the different grains are ordered randomly with respect to one another [18]. Within thin films, on the other hand, surface and interfacial energetics become increasingly important, resulting in domains with a much higher degree of ordering and orientation. These surface and substrate boundary conditions require the most energetically favourable block reside at a given boundary, while still minimizing the amount of interface between A and B segments. Furthermore, as film thickness is

decreased commensurability has much larger consequences over how the film accommodates its characteristic domain lengthscale within the thickness of the film. Geometries which confine the diblock system in 2 or 3 dimensions, even beyond the 1 dimensional confinement of a simple thin film, can result in a range of interesting morphologies not seen in the bulk [19]. Thus, a consideration of the constraints relevant to block copolymer thin films can result in more complex ordered structures than what might be found in similar bulk samples.

Boundary conditions play an important role in the morphology of thin film diblock systems. *Symmetric wetting* refers to the condition when the same block segment resides at both boundaries [18]. This would be the case for systems under confinement where both surfaces are capped with the same substrate. More common though, particularly for engineering applications, is when the surface and substrate energetics are quite different (for example, a film on a Si substrate with an air interface at the free surface). This situation often results in *asymmetric wetting*, where a different block resides at each boundary [18]. In some cases, the interfacial energy at the substrate compared to the surface interaction energy can differ by an order of magnitude [20]. Such asymmetries can have a huge affect on morphology, particularly as films get thinner. One of the most commonly studied thin film systems is the lamellar forming block copolymer [20]: for thicknesses greater than the characteristic domain spacing, lamellae form parallel to the substrate, with the block which has the more favourable interaction at the substrate and the block with the lower surface energy at the free surface. However as the film thickness becomes less than the characteristic domain thickness, the film adopts a perpendicular lamellar morphology since parallel lamella would require the chains be compressed to a high degree. The perpendicular morphology maximizes the system's conformational entropy. Tuning the film thickness and surface-polymer interactions within confined thin films can affect chain conformational entropy and the free energy of the confined system, resulting in varying lamellar morphologies depending on the exact conditions [21]. Thus, thin film block copolymer systems exhibit a morphology thickness dependence which is not seen in the bulk. Studies have predicted a range of morphologies

depending on thickness including "hybrid" structures, such as films incorporating both parallel and perpendicular lamella and cylinder arrangements [18, 22, 23,24]. Most of this work centres on diblocks of symmetric volume composition. Polymers with asymmetric composition have more complex parameters, requiring larger computational power. There is a need for a larger theoretical framework for non-symmetric thin film diblock systems.

## 1.5 Crystallisation within Block Copolymers

Semicrystalline block copolymers (copolymers with one or more block capable of crystallisation) have been the focus of considerable experimental attention. The competition between crystallisation and inter-block incompatibility drives self-organization, resulting in complex ordered structures. In particular, when the crystal block is the minor component, crystallisation may be restricted within nanoscaled microdomains, allowing for the study of crystal confinement. There are currently numerous reviews detailing the current progress as well as open areas in the study of crystallisation within semicrystalline block copolymer systems[25 -27] and in polymers in general [28, 29].

The kinetics of crystallisation actually involves two separate processes, crystal nucleation followed by subsequent crystal growth. Thus the total crystallisation rate will depend on the respective rates of both. Usually, the growth rate is much faster than that for nucleation. This makes it difficult to measure nucleation rates in bulk samples. Once crystal nuclei have formed, the growth of crystal spherulites quickly takes over until the bulk of amorphous material has become crystalline. Thus, the growth kinetics are usually too fast to allow for enough nucleation events to take place within the sample for an adequate measure of the nucleation rate. For this reason, bulk studies typically focus only on crystal growth rates.

Through careful choice of sample geometries, however, it is possible to access the nucleation rate by dividing the polymer sample into small compartments. Provided they are well isolated from one another, crystallisation can occur independently within each domain. Furthermore, if the domains are small enough, once a crystal is nucleated within, there is very little material left for growth to take place. Thus, the time scale for crystal growth is much smaller than for nucleation [11]. The small domain size also implies that in a single sample, there is a large ensemble of domains, each capable of crystallising. In this way, it is possible to study nucleation rates independent from crystal growth.

Experimentally, this compartmentalisation can be easily achieved through block copolymers and dewetted droplet systems. For block copolymers, the minority block can be chosen to be semicrystalline, thus achieving crystallisable isolated domains with nanometre lengthscales, once the material phase-separates. In particular, the domains are relatively monodisperse given the regularity of the chain block lengths. In previous work, we were able to demonstrate the success of the dewetting technique [11]. A thin film of poly(ethylene oxide) was cast onto a thick poly(styrene) film, which is an energetically unfavourable substrate. Upon annealing the films, holes in the PEO layer formed and subsequently grew so as to minimize the unfavourable substrate interaction, leaving behind a system of isolated, dewetted droplets of varying domain size. This technique benefits from the versatility with which the range of droplet sizes can be controlled through the initial film thickness. The study done for this thesis achieves nanometre-scaled domains through the use of a block copolymer system.

Confined crystallization in a semicrystalline-glassy block copolymer was first described by Lotz and Kovacs [7] in an asymmetric poly (ethylene oxide)-b-polystyrene and later investigated by Robitaille and Prud'homme [30]. Large undercoolings were required to initiate crystallisation, suggesting a homogeneous nucleation mechanism. In general, when crystallisation is confined to domains on a nanometre length scale, the kinetics are drastically different from bulk samples. Nucleation is thought to occur homogeneously, since the number of domains is far greater than the number of defects which usually serve as heterogeneous nucleation sites in bulk homopolymer systems. For

these systems, where crystallisation is driven by a homogeneous mechanism, the rate is proportional only to the number of domains yet to be crystallised [7-10, 26].

Deviation from this behaviour occurs when confinement is not strong enough to contain crystallisation. Studies have shown that when the matrix was rubbery as opposed to glassy, crystallisation could break out and destroy the phase-separated melt morphology [26, 31-34]. However, if the blocks are strongly segregated, this may not be the case, and the phase-separated morphology can be preserved upon crystallisation [9]. Chen and co-workers found they could increase confinement by blending poly (butadiene-b-ethylene oxide) (PB-PEO) with a low molecular weight PB homopolymer [10]. Increasing the homopolymer volume fraction in this way yielded lamellar, cylindrical and spherical morphologies, depending on the initial volume fraction and the amount of homopolymer added.

Previous studies of semicrystalline block copolymers have employed a range of techniques to probe kinetics, with differential scanning calorimetry (DSC) being the most commonly utilised [9,10,26,30,34-36]. Morphological details in semicrystalline block copolymers can be quantified with small and wide angle X-ray scattering (SAXS and WAXS) in bulk samples [9,10,30,35], while X-ray reflectivity can resolve structural detail in thin films [37]. Microscopy has long been a useful tool for examining morphology and structure, either by electron or optical techniques [9,11,35]. Atomic force microscopy (AFM) studies by Reiter and co-workers have allowed for direct visualisation of nucleation within individual spherical domains of thin PB-PEO films [8]. The use of AFM was particularly insightful because the random distribution of nucleated domains verified that crystallisation was occurring in each sphere, independent of neighbouring sites.

In the first part of the work presented in this thesis, ellipsometry is employed to study crystallisation in thin films of poly(butadiene-b-ethylene oxide) (PB-PEO). This diblock copolymer phase-separates into crystallisable PEO spheres embedded in a rubbery PB matrix. To the best of our knowledge, the use of ellipsometry to characterize crystallisation in polymer films is novel. Ellipsometry is a well suited probe for

crystallisation within sphere-forming block copolymer systems. Through spincasting, it is straightforward to make thin films that are suitably uniform for ellipsometry. The footprint of the laser beam on the sample is on the order of millimetres, whereas a typical spherical domain is on the nanometre length scale. Thus, in a single experiment, millions of domains are probed, each acting as a separate experiment in its ability to nucleate independently. Furthermore, the film can still be approximated as an isotropic medium because we are averaging over many domains almost two orders of magnitude smaller than the wavelength of the light used to probe them.

In the second part of this work, ellipsometry is used to characterize a morphological transition that occurs in this PB-PEO diblock system. Such a transition has yet to be observed in other experiments. Thus, through both parts of this work, we aim to demonstrate the versatility of ellipsometry in its ability to study aspects of block copolymer systems including crystallisation and morphological transitions.

# Chapter 2

# Experimental Details

This chapter discusses the techniques utilized to prepare and analyse the diblock films under study. Methods of sample preparation are presented in detail as well as a description of the ellipsometry technique and apparatus used to gather data for analysis.

## 2.1 Sample Preparation

### 2.1.1 Solutions and Spincoating

In this study, thin films of poly (1-4 addition butadiene-b-ethylene oxide) (PB-PEO) were prepared by spincasting from solution. All polymer was purchased from Polymer Source, Inc (Dorval Quebec, Canada). Two PB-PEO copolymers were compared which differed only in the length of the PEO chain. These were PB-PEO ($M_{n,PB}$ = 26 000 g/mol, $M_{n,PEO}$ = 6.8 kg/mol, $M_w/M_n$ = 1.06) and PB-PEO ($M_{n,PB}$ = 26 kg/mol, $M_{n,PEO}$ = 4.5 kg/mol, $M_w/M_n$ = 1.06). Due to the large asymmetry in volume fraction of these diblocks, they are sphere-forming systems, with minority PEO spheres embedded in a PB matrix. The larger PEO block has a sphere radius of 12.5 nm [38], while the smaller block has a sphere radius of 8.3 nm [39]. The PB-PEO diblocks were blended with polybutadiene homopolymer (PB) ($M_n$ = 1.1 kg/mol, $M_w/M_n$ = 1.14, 1-4 addition) to inhibit domain coalescence upon crystallisation [38]. The molecular weight of the PB homopolymer is much smaller than the PB block molecular weight to ensure wet-brush blends.

The PB-PEO/PB blends were prepared by dissolving both the PB-PEO diblock and PB homopolymer in toluene such that the total polymer content of the solution was comprised of 20 % PB homopolymer by weight. Solutions were heated for approximately 4 hours at 70 °C to fully dissolve the polymer, and then filtered with Millipore filters (0.2 $\mu$m pore) to remove larger contaminants. Solutions were always allowed at least 24 hours after preparation to mix before being used to ensure complete mixing had occurred.

Films were spincast onto clean Si substrates by the "drop-then-spin" method, where a drop of solution is placed on the substrate with a pipette, and subsequently spun. This was preferred over the "spin-then-drop" method of spincoating, where a drop of solution is released onto the centre of the substrate after the substrate has already begun spinning. The "drop-then spin" method resulted in films which were more uniform in colour, indicating a more constant thickness over the substrate. This was important for the purpose of ellipsometry, as measurements would be sensitive to slight thickness variations in the film. Furthermore, the data analysis method assumes a constant film thickness, thus it is important that the films be as uniform as possible to better meet this assumed condition.

A range of film thicknesses were investigated in this study. This was accomplished in two ways. First, solution concentrations were varied from 1% to 4% PB-PEO/PB by weight, allowing for course changes in thickness. Secondly, for a given solution concentration, spin speeds were varied between 1500 to 5000 rpm, allowing even finer thickness adjustments. In this way, films with thicknesses $35 < h < 220$ nm were prepared.

### 2.1.2 Substrates

For all samples, Silicon (Si) substrates were used. Polished Si wafers (100 orientation) with an approximately 3 nm native oxide layer were obtained from University Wafer and cleaved into 9 mm squares. Care was taken in the cleaving process to minimize the amount of Si dust created, in the interest of keeping the substrate surface as contaminant

free as possible. Prior to spincoating, the Si substrates were solvent cleaned by spincoating Milli-Q water followed by methanol onto the substrate repeatedly at ~ 5000 rpm. The Si was then UV ozone treated for approximately 60 min to remove organic contaminants.

### 2.1.3 Annealing

After preparation of the PB-PEO/PB films, samples were annealed either in vacuum or in a dry nitrogen environment for at least one hour at a temperature of 90 °C. This allowed for the removal of excess solvent trapped within the film, the removal of stresses in the chains induced by spincoating, as well as allowing for phase-separation to take place. It was important that annealing take place either in vacuum or nitrogen, as PB is highly reactive in air, particularly at elevated temperatures. In air, there is a certain probablility for the carbon double bond in the PB block to break resulting in a structure closer to poly(ethylene).

The annealing temperature chosen is above the melting temperature for bulk PEO ($T_m$ ≈64 °C) and the glass transition temperature of 1-4 addition PB ($T_g$ < -40 °C) [40], while being well below ODT for PB-PEO ($T_{ODT}$ > 220 °C) [41]. One hour was sufficiently long enough to allow the phase-separated morphology consisted of PEO minority spheres in a PB matrix to form, as verified by AFM.

## 2.2 Sample Characterisation

### 2.2.1 Ellipsometry

Ellipsometry measures changes in polarisation of elliptically polarised light upon reflection from a film-covered substrate to enable calculation of the refractive index and thickness of the film [42]. In a nulling ellipsometer, light from a laser is passed through a quarter wave plate and a polariser at an angle such that it is elliptically polarised before it

reaches the sample but linearly polarised upon reflection. The light then passes through a second polariser (called the analyser) which is oriented such that all light is extinguished. The ellipsometric setup is shown schematically in Figure 2.1. The polariser and analyser angles ($P$ and $A$) can be inverted to calculate film thickness, $h$, and refractive index, $n$, *assuming an isotropic film*. By monitoring the temperature dependence of these quantities, we can observe the densification associated with crystallisation.

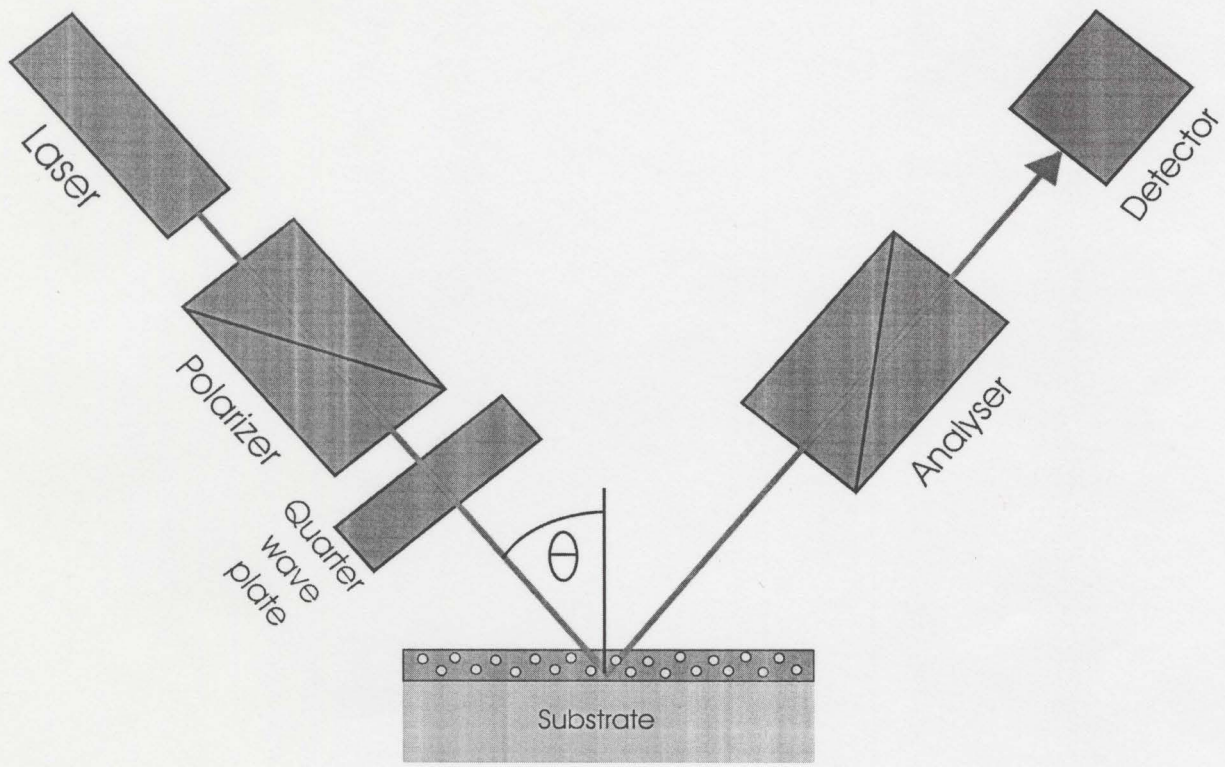


Figure 2.1: Schematic of ellipsometric setup. Laser light is passed through a polariser and quarter wave plate, reflected from the film-covered substrate, and then passed through an analyser before arriving at the detector. The polariser and analyser angles are oriented such that a null is detected. The values of these angles at null may be used to calculate film thickness and index of refraction.

For the measurements, a custom built single wavelength self-nulling ellipsometer was used. The design of this ellipsometer enables measurement of $P$ and $A$ values to 0.0001°. Temperature was controlled to 0.1 °C with a Linkam THMS 600 stage, and cooling accomplished with a Linkam LNP94 liquid nitrogen pump cooling system. Once the sample was mounted on the hotstage, the sample chamber was flushed with nitrogen to ensure a dry atmosphere at all times. Samples were annealed at 70 °C for a few minutes before being cooled to -30 °C, held there for 30 minutes, and then heated to 70 °C. In all experiments presented here, heating and cooling was carried out at 1 °C/min, unless otherwise stated. This rate was chosen as a good compromise between slow enough kinetics to allow for the collection of large amounts of data and a reasonable time limit for the length of a single experiment. After the temperature run was complete, the measured polariser and analyser null angles were inverted to film thickness and refractive index values using the standard equations of ellipsometry [42].

# Chapter 3

# Results and Discussion

## 3.1 Ellipsometry and Crystallisation

The versatility of ellipsometry complements information gained through other techniques. The study presented in this thesis is analogous to what is done in a typical DSC measurement, however ellipsometry allows for the study of thin films (volumes ~ $10^{-10}$ L). AFM has proven to be a very useful tool in thin film studies [8], though *dynamic* experiments are challenging, and typically DSC requires fairly fast heating and cooling rates (~ 10 °C/min). In contrast, ellipsometry is capable of both dynamic and isothermal experiments, which can serve to complement understanding gained through AFM and DSC. Furthermore, with ellipsometry we have the ability to use quick temperature ramp rates (~ 50 °C/min), or rates as slow as one is willing to wait. The ability to carry out isothermal and dynamic experiments on very small volumes makes ellipsometry a versatile tool for the study of crystallisation.

In order to study homogeneous nucleation in confined spherical domains of a phase-separated block copolymer, the melt morphology must be preserved upon crystallisation. For the PB-PEO/PB films used in this study, the glass transition temperature of the PB matrix is well below crystallisation temperatures, which means the PB matrix is in the rubbery state for the temperature range accessed. However, as Chen and co-workers demonstrated, this diblock is strongly segregated, with confinement

further strengthened by the presence of the PB homopolymer [10]. Thus, crystallisation is effectively confined within the spherical domains without breakout or domain coalescence occurring when crystallisation temperatures are reached.

The results of a typical ellipsometry experiment are shown in Figure 3.1. The polariser and analyser angles that result in a null at the detector are measured as a function of temperature, $T$, which are converted to measures of thickness and index of refraction. The example shown in Figure 3.1 is the larger PEO block sample, however it should be noted that while quantitative features vary, the basic qualitative features of the thickness and index plots are the same for both block lengths.

A novel feature of using ellipsometry for the study of block copolymer crystallisation, is the ability to measure changes in the film's coefficient of volume expansion ($\alpha$) due to crystal-related thermal transitions from plots of $h$ versus $T$ (see Figure 3.1(c)). As the sample was cooled from 70 °C to -21 °C, it is observed that the PB melt matrix and the PEO supercooled melt contract at a constant rate ($\alpha = (7.3 \pm 0.2) \times 10^{-4}$ K$^{-1}$). At -21 °C, the film suddenly undergoes a rapid contraction (over a range of approximately 5 °C) as the spheres begin to crystallise. The onset of crystallisation is consistent with temperatures measured for nucleation within similar sized spherical domains of PEO [8]. The rapid contraction at -21 °C is precisely what one should expect: as each domain crystallises, it densifies, thus reducing the average thickness of the film. This densification is also reflected in the sudden increase in refractive index over this temperature range. It is noted that throughout the experiments, the PB matrix remains in the melt state, so changes in the expansion coefficient are the result of a phase change in the PEO block. The PB-PEO expansion coefficient is consistent with what is observed for PB ($\alpha = (6.8 \pm 0.2) \times 10^{-4}$ K$^{-1}$) and PEO ($\alpha_{amorphous} = (7.3 \pm 0.2) \times 10^{-4}$ K$^{-1}$) homopolymer [43]. After crystallisation is complete, the film is seen to contract with a smaller coefficient ($\alpha = (6.6 \pm 0.2) \times 10^{-4}$ K$^{-1}$), as reflected in the smaller slope in Figure 3.1(c) after nucleation when compared to the slope before nucleation. Upon heating, the film expands with this new expansion coefficient until it reaches a temperature of approximately 50 °C. At this point, a rapid expansion is seen as the crystal domains melt

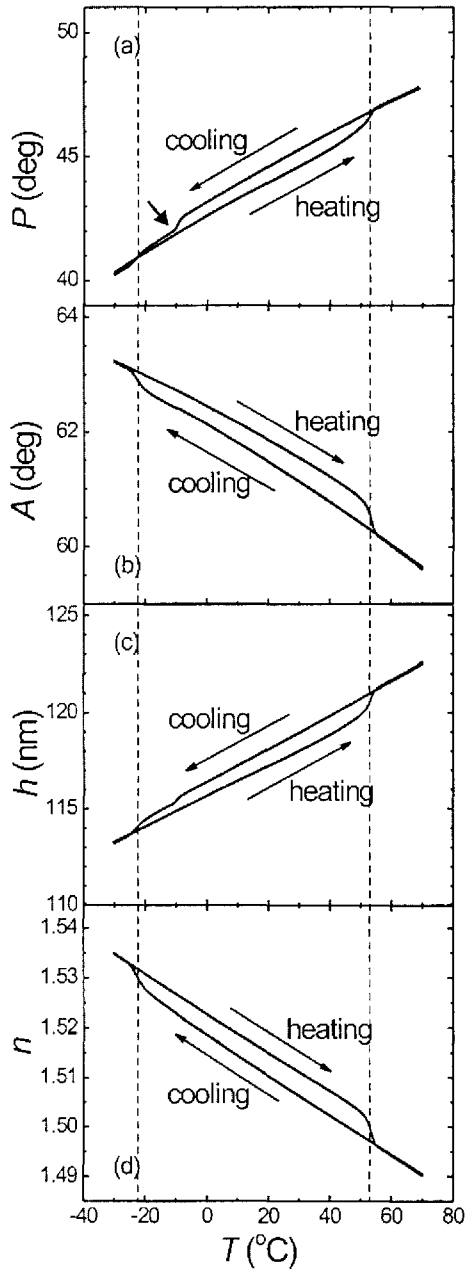


Figure 3.1: The results of a typical ellipsometry crystallisation experiment where we have plotted: a) polariser angle, b) analyser angle, c) film thickness, and d) index of refraction, versus temperature. The lack of scatter or drift in the data reflects the extreme sensitivity of the ellipsometer measurement. The linearity of the slopes in (c) and (d), despite the curvature of the plots in (a) and (b), indicates that treating the diblock as a uniform film is a good approximation. The arrow in (a) inicates a deviation in the plots, which will be discussed in section 3.2.

(over approximately 5 °C), with a corresponding decrease in refractive index. Once all the domains have melted, $\alpha$ returns to its initial value, since the material is completely amorphous again.

It should be noted that during cooling, a deviation can be seen in the plots in Figure 3.1 around -10 °C (see Figure 3.1(a)). Subsequent experiments have shown that this deviation is neither an artifact nor related to crystallisation. The nature of this deviation will be discussed in section 3.2.

The large supercooling ( $\approx$ 80 °C) required to initiate crystallisation is characteristic of homogeneous nucleation [8,10]. The transition occurs over a 5 °C range, which is expected since each domain must create its own nucleus, a process that has been shown to occur stochastically [8, 11]. In agreement with the findings of Röttele and co-workers, a wide temperature range ( $\approx$5 °C) is observed over which melting occurs. This has been attributed to the fact that individual domains exist in various metastable states, having been formed under such large supercoolings. As a result, domains melt at different temperatures, depending on the extent of stability and reorganization within each individual domain [35].

In addition to demonstrating the success of ellipsometry in studying nucleation in block copolymer systems, the crystallisation and melting temperatures of two different diblocks have been compared. In earlier work, we investigated how the nucleation rate scales with domain size [46]. For that study, a unique sample geometry of dewetted PEO droplets on an unfavourable polystyrene substrate was used [11]. It was possible to show that there is a volume dependence on the homogeneous nucleation rate. Given that homogeneous nucleation is a random process, equally likely to occur in any compartment, domains with more material nucleate on average at higher temperatures. For this study, two diblocks which differ only in the length of the PEO block were compared. Given the uniformity of domain sizes in phase separated block copolymers, this is an ideal system for a volume comparison of the crystallisation kinetics between the two diblocks.

In Figure 3.2 is a plot of: a) the crystallisation temperature, $T_c$, and b) the melting temperature, $T_m$, versus the sphere radius, $R$, for several films of the two PEO block

lengths. It is found that the longer block length samples ($R \approx 12.5$ nm) crystallise and melt at higher temperatures than the shorter PEO block samples ($R \approx 8.3$ nm). The change in $T_c$ with $R$, shown in Figure 3.2(a), is consistent with our previous findings for larger volume droplets where homogeneous nucleation was found to scale with the volume of the domain [46].

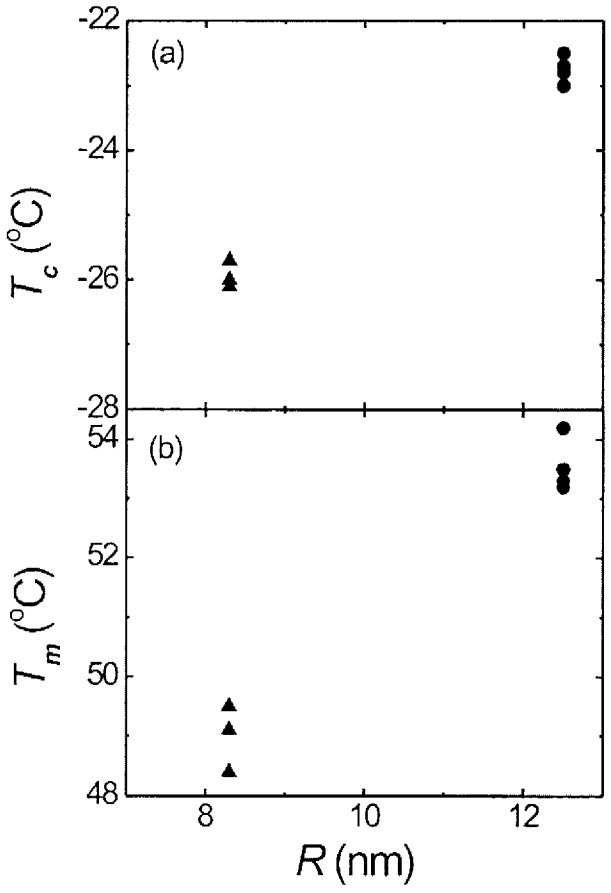


Figure 3.2: Plot of: a) crystallisation temperature, $T_c$, and b) melting temperature, $T_m$, versus domain radius, $R$. Triangles represent the smaller PEO block length ($M_{n,PEO}$ = 4.5 kg/mol) and circles represent the larger PEO block length ($M_{n,PEO}$ = 6.8 kg/mol).

Generally, crystals that are nucleated at larger supercoolings experience faster growth rates than those which nucleate at higher temperatures. As a result, the crystals formed at the lower temperatures are less stable than their higher temperature counterparts. Since they contain more defects, less stable crystals should melt at a lower temperature than more stable crystals. In Figure 3.2(b), a decrease in $T_m$ with domain size $R$ is seen (by ~ 1 °C/nm for the two samples presented), which is consistent with previous results in sphere forming domains [36]. This is not surprising since the crystals within the smaller spheres are less stable than larger domains.

## 3.2 Ellipsometry and Diblock Ordering Transitions

As was commented in the previous section, a deviation can be seen in Figure 3.1 around -10 °C while cooling the film. It was verified that this deviation is not the result of some crystallisation phenomena, such as heterogeneous nucleation, for example. To see this, a film was subjected to the usual thermal treatment (cooled to -30 °C so as to allow for crystallisation after ≈-21 °C), followed by subsequent heating. After this initial thermal treatment, the film was then cooled again, however this time only to 0 °C, held there for 10 minutes and heated back up. These results can be seen in Figure 3.3, where the data from both experiments have been superimposed on one another. The lighter data corresponding to the latter thermal treatment has been shifted to either side of the first thermal treatment (black data) to aid in the comparison of the two experiments. It should be noted that for the rest of this section, the longer PEO length diblock was used in all experiments, though similar results were observed for the shorter block length. From Figure 3.3, it can be seen that while both curves experience the deviation at ≈10 °C, differences can be noted between the two curves. As was explained previously, the black data shows a change in slope after crystallisation (at ≈-21 °C) due to the fact that the material now has a smaller expansion coefficient on account of being partially crystalline. If one examines the slopes before and after the deviation in the lighter curve, it can be

seen that no such change in expansion coefficient takes place; the slopes before and after the deviation are the same within experimental error. This suggests that the deviation is not caused by crystallisation, since one would expect this to be accompanied by a decrease in $\alpha$.

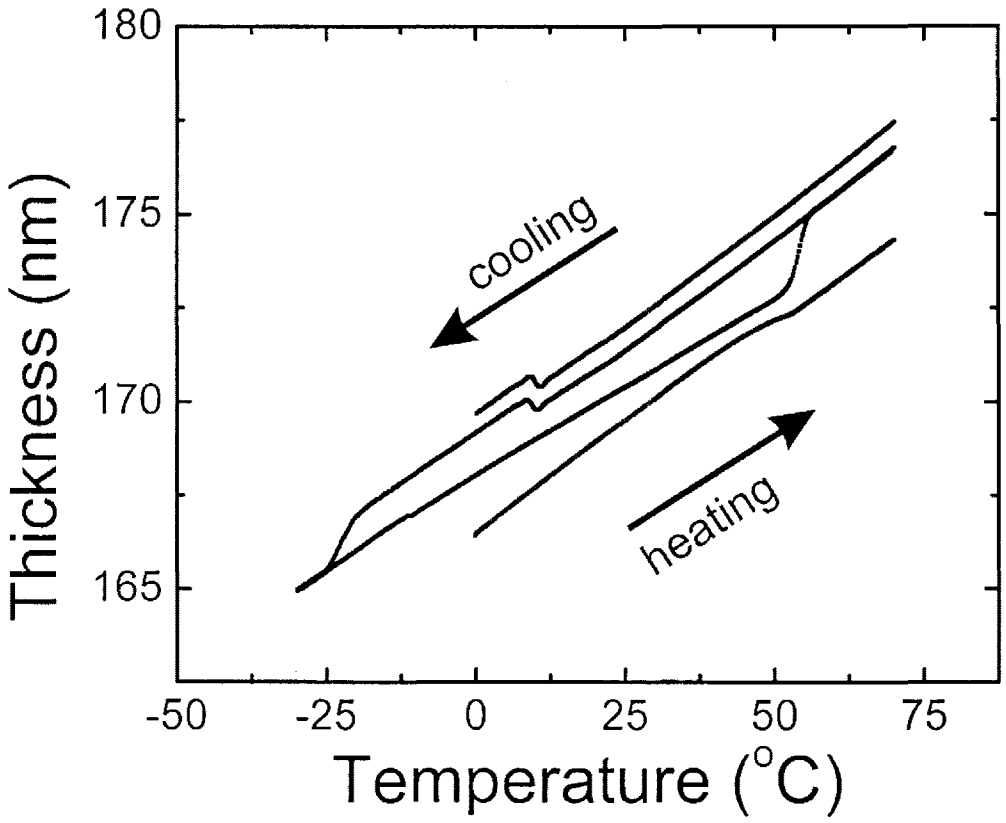


Figure 3.3: The results of two separate thermal runs differing only in temperature the film is cooled to. The black curve has undergone the usual thermal treatment, having been cooled to -30 °C. The lighter curve has been cooled only to 0 °C. This curve has been shifted above and below the black curve to aid in their comparison. It can be seen that the lighter curve does not experience a change in expansion coefficient at any temperature, as evidenced by its slope, unlike the black curve which experiences changes in $\alpha$ after crystallisation (at $\approx$-21°C) and again after melting (at $\approx$55°C) .

The experimental evidence suggests the origin of the deviation is related to diblock ordering rather than crystallisation. The system described in this study, being substrate supported with a free surface, experiences asymmetric boundary conditions and asymmetric wetting. It is known that the PB block has a lower surface energy than PEO resulting in a PB layer residing at the surface [47]. From wetting/dewetting experiments, we know that the PEO block has a greater affinity for the Si substrate, and thus prefers to wet the substrate interface over the PB block. Furthermore, this is a block copolymer with composition such that a sphere forming morphology is energetically favourable. Thus, the film must satisfy all these constraints at the same time within the confines of the thin film. It should be expected that the frustration this leads to results in interesting morphological phenomena. As pointed out by Matsen, while cylinder and sphere forming block copolymer thin films have not received much theoretical attention, rich morphological behaviour should be expected, particularly when the minority block is attracted to the substrate [24].

Evidence that the deviation may be caused by a morphological transition can be found in a comparison between the experimental data and ellipsometry data that we have simulated. We first describe the assumed transition in the morphology and will then proceed to show that this is consistent with our measurements. Initially, when the film is at 70 °C, the film consists of a homogeneous layer of ordered spheres on the Si substrate. Due to the high affinity for PEO to wet the substrate, there is a layer of "partial" spheres at the substrate, known as a *partial wetting layer*, as depicted in Figure 3.4(a). As the temperature is lowered, we approach a point where this morphology is no longer the most energetically favourable, as will be discussed below, and the film undergoes a transition such that the layer of "half" spheres form a lamellar layer of PEO at the substrate instead, referred to as a PEO *wetting layer* (see Figure 3.4(b)).

Evidence for this transition may be found in Figure 3.5, where the results of experiment and simulation respectively can be compared. To understand the plots in this figure, it should first be noted that in order to convert $P$ and $A$ values to $h$ and $n$, a single,

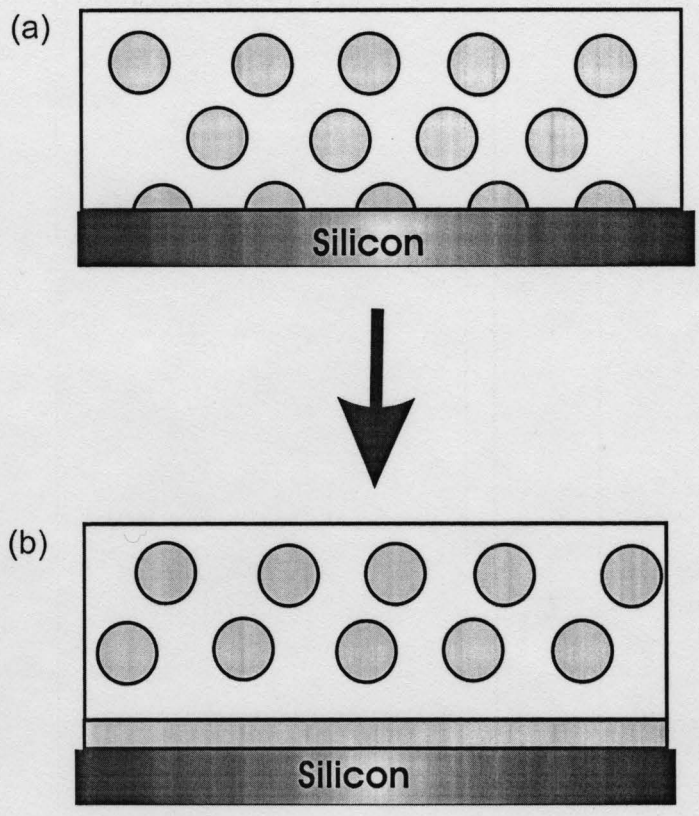


Figure 3.4: Schematic of the transition. As homogeneous ordered film of PEO spheres within a PB matrix (top image) is cooled, (a) "half" layer of spheres at the substrate *(partial wetting layer)* reorders into (b) lamellar layer (*wetting layer*) such that the PEO block fully wets the substrate (lower image).

uniform film model is assumed. From plots of $h$ and $n$ versus $T$, a net change in $h$ and $n$ can be seen at the deviation. For different film thicknesses, this results is either a net increase or decrease, with $n$ usually experiencing the opposite behaviour to $h$ (ie: if $h$ undergoes a net increase as a result of the deviation, than $n$ experiences a net decrease). A range of film thicknesses ($35 < h < 220$ nm) were prepared to investigate the effect of film thickness on the deviation. Thus, in Figure 3.5(a), the *change in h and n* that takes place at the deviation is plotted versus film thickness. From these plots, it is seen that these changes follow a smooth curve.

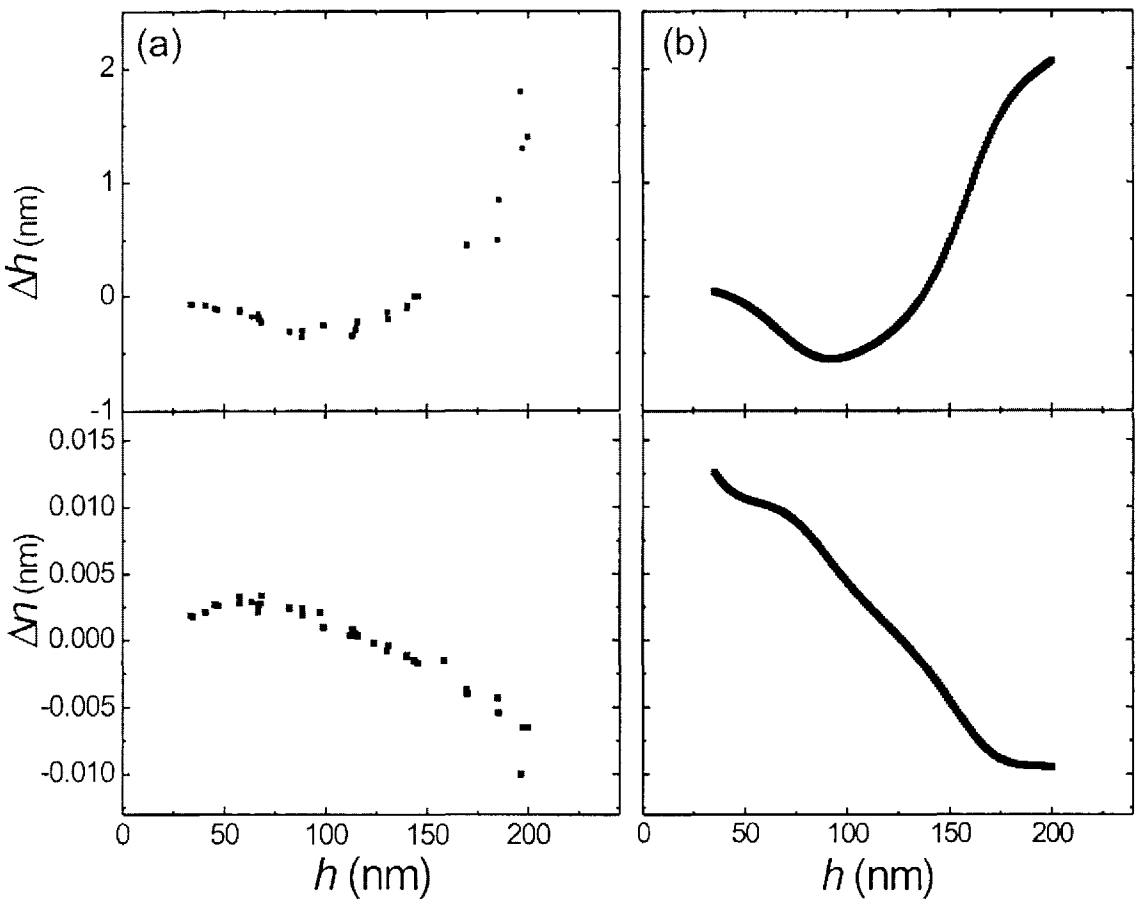


Figure 3.5: Changes in thickness and refractive index versus film thickness at the deviaiton: (a) measured experimentally and (b) with simulated elipsometry data. In (a), both $h$ and $n$ plots are seen to follow smooth curves. In (b), ellipsometry data is simulted assuming (1) a homogeneous film on a Si substrate and (2) a homogeneous film with a 12 nm layer at the Si substrate. Plots show simulated $h$ and $n$ values from (2) subtracted from those simulated from (1) respectively plotted versus film thickness. The $h$ and $n$ curves in (b) are very similar to those in (a).

To understand Figure 3.5(b), it is noted that using the standard equations of ellipsometry and reasonable values for substrate and film refractive indices, it is possible to simulate $P$ and $A$ (and thus $h$ and $n$) values for various sample geometries. This was done for two different geometries: (1) a homogeneous film with refractive index comparable to the measured value for a PB-PEO/PB diblock film, on a substrate with parameters equivalent to Si, and (2) the same conditions as in (1) however now with a 12 nm layer of a film with refractive index comparable to PEO sandwiched between the substrate and homogenous film. A 12 nm layer was chosen as a crude estimate since this is the radius of the PEO minority spheres for the PEO block used in these experiments. For both sets of data, values for thicknesses of 35 to 200 nm were generated in increments of 1 nm. The simulated values for $h$ and $n$ from data set (2) were then subtracted from data set (1) and respectively plotted versus film thickness. These plots are displayed in Figure 3.5(b). One can see that the plots in Figure 3.5(b) agree qualitatively with the plots in Figure 3.5(a). Both share the same curve shapes, with inflection points occurring at approximately the same thicknesses, and relative agreement between the ranges of $\Delta h$ and $\Delta n$ plotted. This indicates that Figure 3.5(a) is actually an artifact arising from the assumptions made in analysing the data. In the analysis of the experimental data, it was assumed that for all temperatures, there was a homogeneous film present. The agreement within Figure 3.5 (a) and (b), however, confirms the picture presented in Figure 3.4, that initially there is only a homogeneous film of ordered spheres present, with a transition upon cooling to a film with a lamellar PEO layer sandwiched between the homogeneous ordered film and the substrate. In the data analysis, it is assumed that there is a single, uniform film present, however, this is only true for the situation depicted in Figure 3.4(a). This assumption becomes inadequate once the PEO lamellar layer is formed. The technique of ellipsometry is so sensitive that it is able to detect the slight change in refractive index that occurs upon forming this lamellar layer. This induces an error in the analysis when this layer is not accounted for which shows up as a change in thickness and index of refraction at the deviation in plots of $h$ and $n$ versus $T$.

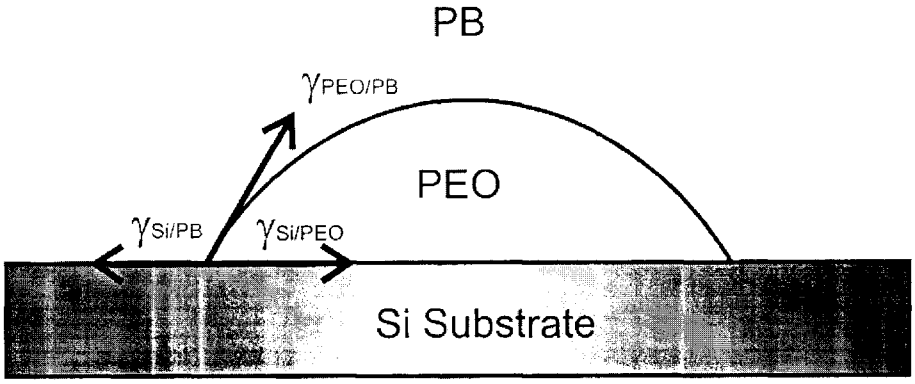


Figure 3.6: Schematic of partial wetting morphology of PEO half-sphere on Si within a PB matrix. Here, $\gamma_{Si/PEO}$, $\gamma_{Si/PB}$, and $\gamma_{PEO/PB}$ represent interfacial tensions of the Si/PEO, Si/PB and PEO/PB interfaces respectively. The balance of these tensions determines whether partial wetting or total wetting is more energetically favourable.

The actual origin of the transition from a PEO partial wetting layer to a PEO wetting layer at the substrate can be understood through an interfacial tension argument. Consider the situation depicted in Figure 3.6, where a spherical drop of PEO is at the Si interface within a PB matrix. $\gamma_{Si/PB}$, $\gamma_{Si/PEO}$, and $\gamma_{PEO/PB}$ are the respective interfacial energies. Strictly from an interfacial tension point of view, a thin PEO wetting layer will always result in a lower free energy if:

$$\gamma_{Si/PB} > \gamma_{Si/PEO} + \gamma_{PEO/PB}; \tag{3.1}$$

since this implies that having PB reside at the Si interface is the more energy costly morphology. From wetting/dewetting experiments performed by us, it is known that PEO prefers to wet the Si substrate:

$$\gamma_{Si} > \gamma_{PEO} + \gamma_{Si/PEO}; \tag{3.2}$$

while PB can dewet on Si:

$$\gamma_{Si} < \gamma_{PB} + \gamma_{Si/PB}; \tag{3.3}$$

From equations (3.2) and (3.3), it follows that:

$$\gamma_{PB} + \gamma_{Si/PB} > \gamma_{PEO} + \gamma_{Si/PEO}. \tag{3.4}$$

Upon rearranging equation (3.4), we have:

$$\gamma_{Si/PB} > \gamma_{Si/PEO} + \gamma_{PEO} - \gamma_{PB}; \tag{3.5}$$

However, given that $\gamma_{PEO}$ = 43mN/m [48], $\gamma_{PB}$ = 35.4 mN/m [49], and interblock interfacial tensions are generally quite low (~ 1 mN/m), we have:

$$\gamma_{PEO/PB} < \gamma_{PEO} - \gamma_{PB}. \tag{3.6}$$

Substitution of (3.6) into (3.5) reveals that equation (3.1) is valid. Thus, from strictly interfacial tension considerations, a PEO wetting layer (Figure 3.4(b)) is preferred at the substrate over the partially-wetted droplet scenario (Figure 3.4(a)). Clearly, however, interfacial tension is not the only consideration in block copolymer phase-separated morphologies. One also has to consider the affects of entropy and chain stretching. In general, the S phase is preferred over the L phase for diblocks of severely asymmetric composition, since the S phase results in a satisfactory degree of chain stretching for both blocks. Therefore, when stretching is a dominating factor, a curved interface is preferred, like the partial wetting case. As one goes to lower temperatures, however, it is known that entropy contributions to the free energy ($-TS$) and thus chain stretching becomes less important. Therefore, there will be a point where interfacial tension becomes dominant in comparison to entropy, thus allowing a transition to a wetting layer. This transition will take place at the point where the free energy for the lamellar layer condition matches the free energy for the partial wetting condition.

To the best of our knowledge, the occurrence of such a transition from a partial sphere to a lamellar layer at the substrate has yet to be observed in experiments. This is likely due to the fact that the techniques usually used to probe thin film diblock kinetics would be unable to detect such a slight transition occurring at the substrate easily. AFM can only probe the surface. DSC studies on thin films are challenging and evidence for the transition would likely be lost in the noise of the measurement. In particular, slow cooling rates would be required to best capture the deviation and it is known that with DSC, the trade-off for using slower rates is an increase in noise. Ellipsometry on the other hand is extremely sensitive to the slightest changes in refractive index and thus can detect such a transition quite easily.

One should expect that the precise temperature the transition takes place at should be affected by the surface energy of the Si substrate. The surface energy will vary depending on the conditions at the time the film was spun (ie; atmospheric humidity, temperature, etc). This seems to be the case for this system if one considers the plot in Figure 3.7, where the temperature of the deviation is plotted versus film thickness. There seems to be a general trend of decreasing temperature with thickness, however there is considerable scatter in the data. This scatter is not due to experimental error. From plots like those of Figure 3.1, one can see how sensitive ellipsometric measurements are for these experiments, with virtually no scatter in the measured data points. The scatter in Figure 3.7 is real, caused by variations in the surface energy of the Si substrate, thus resulting in fluctuations in the temperature at which the transition occurs.

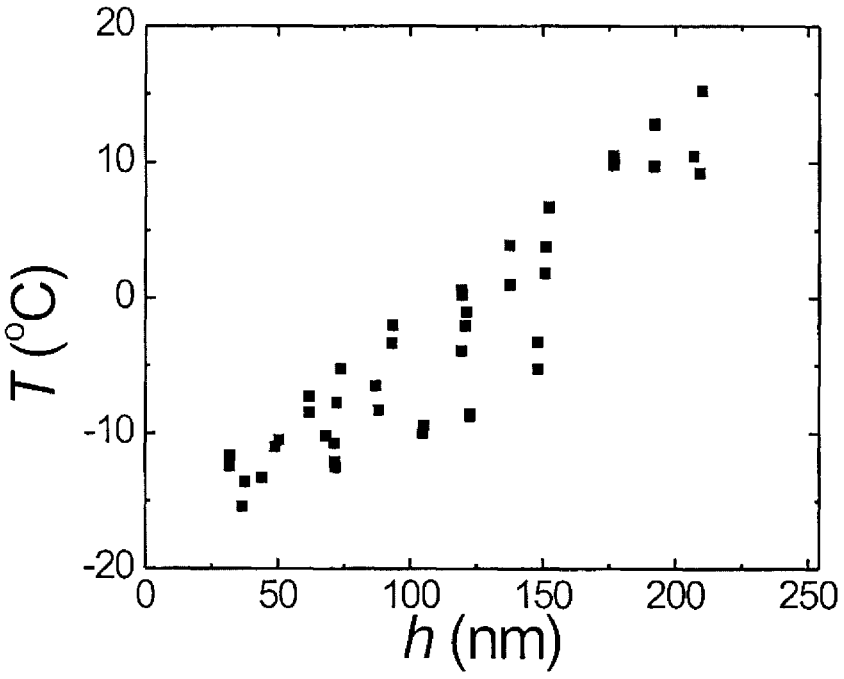


Figure 3.7: Plot of the temperature at which the transition occurs versus film thickness. Significant scatter is seen in the data which is likely caused by fluctuations in surface energy of the Si substrate.

# Chapter 4

# Conclusion

In this study, we have demonstrated that ellipsometry provides a novel probe for the study of crystallisation kinetics and morphological transitions in block copolymer systems, offering valuable insight which complements other techniques currently being employed. We have shown that ellipsometry is sensitive to the variations in crystallisation and melting kinetics that occur with changing domain size in block copolymer films, even for very small sample volumes ($10^{-10}$ L). For the experiments conducted in this study, we were able to obtain expansion coefficients before and after crystallisation. The ability to observe phase transitions through small changes of the density in thin films makes ellipsometry a versatile tool for the study of crystallisation kinetics. Furthermore, it has been shown that ellipsometry is sensitive to very slight changes in refractive index, allowing for the detection of what is believed to be the formation of a lamellar layer at the substrate as the film is cooled. This is particularly insightful as no other current technique being used to study thin block copolymer films can easily follow the kinetics of such a morphological transition. This opens the possibility for future isothermal studies where timescales for this transition can be measured.

# References and Notes


[1] A.Y. Grosberg, and A.R. Khokhlov, *Giant Molecules: Here, There, and Everywhere...*, Academic Press: Toronto, 1997.

[2] U.W. Gedde, *Polymer Physics*, Kluwer Academic Publishers: Dordrecht, 1999.

[3] R.L. Jones, *Soft Condensed Matter*, Oxford University Press: New York, 2002.

[4] J. Israelachvili, *Intermolecular & Surface Forces*, Academic Press Limited: London, 1992.

[5] R.L. Jones, and R.W. Richards, *Polymers at Surfaces and Interfaces*, Cambridge University Press: Cambridge, 1999.

[6] G. Strobl, *The Physics of Polymers: Concepts in Understanding Their Structure and Behaviour, Second Ed.*, Springer-Verlag: Berlin, 1997.

[7] B. Lotz and A.J. Kovacs, ACS Polym. Prepr., **10**, 820 (1969).

[8] G. Reiter, G. Castellein, J.-U. Sommer, A. Röettele and T. Thurn-Albrect, Phys. Rev. Lett., **87**, 226101 (2001).

[9] Y.-L. Loo, R.A. Register and A.J. Ryan, Phys. Rev. Lett., **84**, 4120 (2000).

[10] H.-L. Chen, J.-C. Wu, T.-L. Lin and J.S. Lin, Macromolecules, **34**, 6936 (2001).

[11] M.V. Massa, J. Carvalho and K. Dalnoki-Veress, Eur. Phys. J. E, **12**, 111 (2003).

[12] M.W. Matsen, and F.S. Bates, J. Chem. Phys., **106**, 2436 (1997).

[13] M.W. Matsen, J. Phys.: Condens. Matter, **14**, R21 (2002).

[14] M. Laradji, A.C. Shi, R.C. Desai, and J. Noolandi, Phys. Rev. Lett., **78**, 2577 (1997).

[15] D.A. Hajduk, H. Takenouchi, M.A. Hillmyer, F.S. Bates, M.E. Vigild, and K. Almdal, Macromolecules, **30**, 3788 (1997).

[16] M.E. Vigild, K. Almdal, K. Mortenson, I.W. Hamley, J.P.A. Fairclough and A.J. Ryan, Macromolecules, **31**, 5702 (1998).

[17] J.-Y. Hsu, B. Nandan, M.-C. Chen, F.-C. Chiu and H.-L. Chen, Polymer, **46**, 11837 (2005).

[18] M.J. Fasolka, and A.M. Mayes, Annu. Rev. Mater. Res., **31**, 323 (2001).

[19] B. Yu, P. Sun, T. Chen, Q. Jin, D. Ding, B. Li and A.C. Shi, Phys. Rev. Lett., **96**, 138306 (2006).

[20] M.J. Fasolka, and A.M. Mayes, Macromolecules, **33**, 5702 (2000).

[21] Y. Yin, P. Sun, T. Chen, B. Li, Q. Jin, D. Ding, and A.C. Shi, ChemPhysChem, **5**, 540 (2004).

[22] H.P. Huinink, J.C.M. Brokken-Zijp, and M.A.J. van Dijk, Chem. Phys., **112**, 2452 (2000).

[23] E. Huang, P. Mansky, T.P. Russel, C. Harrison, P.M. Chaikin, R.A. Register, C.J. Hawker, and J. Mays, Macromolecules, **33**, 80 (2000).

[24] M.W. Matsen, J. Chem. Phys., **106**, 7781 (1997).

[25] Y.-L. Loo, *Templating Polymer Crystal Growth on a Nanoscale Using Phase-Separated Block Copolymers*. In *The Encyclopedia of Nanoscience and Nanotechnology*; Marcel Dekker: New York, 2002.

[26] Y.-L. Loo and R.A. Register, in *Developments in Block Copolymer Science and Technology*, I.W. Hamley, Ed., (John Wiley & Sons Ltd., West Sussex, 2004) p. 213.

[27] A.J. Muller, V. Balsamo and M.L. Arnal, *Crystallization in Diblock and Triblock Copolymers*, Advances in Polymer Science, **190**, 1 (2005).

[28] S.Z.D. Cheng and B. Lotz, Phil. Trans. R. Soc. A, **361**, 517 (2003).

[29] S.Z.D. Cheng and B. Lotz, Polymer, **46**, 8662 (2005).

[30] C. Robitaille and J. Prud'homme, Macromolecules, **16**, 665 (1983).

[31] S. Nojima, K. Kato, S. Yamamoto and T. Ashida, Macromolecules, **25**, 2237 (1992).

[32] K. Sakurai, W.J. MacKnight, D.J. Lohse, D.N. Schulz and J.A. Sissano, Macromolecules, **27**, 4941 (1994).

[33] A.J. Ryan, I.W. Hamley, W. Bras and F.S. Bates, Macromolecules, **28**, 3860 (1995).

[34] J.-T Xu *et al.*, Macromolecules, **35**, 3614 (2002).

[35] A. Röttele, T. Thurn-Albrecht, J.U. Sommer and G. Reiter, Macromolecules, **36**, 1257 (2003).

[36] S. Nojima, M. Toei, S. Hara, S. Tanimoto and S. Sasaki, Polymer, **43**, 4087 (2002).

[37] R. Opitz, D.M. Lambreva, and W.H. de Jeu, Macromolecules, **35**, 6930 (2002).

[38] Y.-Y. Huang, C.H. Yang, H.-L. Chen, F.-C. Chiu, T.-L. Lin and W. Liou, Macromolecules, **37**, 486 (2004).

[39] In order to calculate the sphere radius in the smaller block length, we used the strong-stretching theory expression for domain size as described in [21], based on a sphere radius and volume fraction for the longer block length as given in [19].

[40] C. Vasilev, G. Reiter, S. Pispas and N. Hadjichristidis, Polymer, **47**, 330 (2006).

[41] Y.-Y. Huang, H.L. Chen and T. Hahimoto, Macromolecules, **36**, 764 (2003).

[42] R.M.A. Azzam and N.M. Bashara, *Ellipsometry and Polarized Light* (North-Holland Publishing Company, Amsterdam, 1977).

[43] These values for $\alpha$ were measured by ellipsometry on PB and PEO homopolymer. The values are consistent with those quoted for 1-4 addition PB and amorphous PEO in the literature [44, 45 respectively].

[44] O. Okada and H. Furuya, Polymer **43**, *971 (2002).*

[45] *J.E. Mark, Ed. Physical Properties of Polymers Handbook,* American Institute of Physics: New York, 1996.

[46] M.V. Massa and K. Dalnoki-Veress, Phys. Rev. Lett., **92**, 255509 (2004).

[47] C. Vasilev, H. Heinzelmann and G Reiter, Journal of Polymer Science: Part B: Polymer Physics, **42**, 1312 (2004).

[48] Z.Q. Lin, D.H. Kim, X.D. Wu, L. Boosahda, D. Stone, L. LaRose, and T.P. Russell, Adv. Mater., **14**, 1373 (2002).

[49] C.J. Lai, Y.L. Loo, R.A. Register, and P.F. Green, Macromolecules, **38**, 7745 (2005).